Available online at www.sciencedirect.com
ScienceDirect
ELSEVIER
Mechanics of Materials 40 (2008) 66–79
MECHANICS OF MATERIALS
www.elsevier.com/locate/mechmat

Damage mechanics of electromigration induced failure

Cemal Basaran *, Minghui Lin

Electronic Packaging Laboratory, Department of Civil, Structural and Environmental Engineering, University at Buffalo, State University of New York, USA

Received 25 September 2006; received in revised form 26 June 2007

Abstract

Electromigration is a major road block in the pursuit of nanoelectronics and next generation power electronics. The current density in the state-of-the-art microelectronics solder joints is about 10^3 A/cm^2. In the next generation nanoelectronics solder joints this current density is expected to increase by an order of magnitude, at least. In this paper, a new damage mechanics formulation is implemented in a general finite element procedure and used for simulation of solder joints electromigration induced failure. Nonlinear viscoplastic time-dependent nature of the material and current crowding effects are taken into account in the formulation. The model is verified against test data.
© 2007 Elsevier Ltd. All rights reserved.

Keywords: Electromigration; Damage mechanics; Current crowding; Nanoelectronics; Solder joint; High current density

1. Introduction

Electromigration failure in thin film VLSI interconnects (mainly Al and Cu) has been studied since early 1960s. Yet, due to low current density in microelectronics solder joints electromigration was not a major concern. Miniaturization of electronics to nanoscale, makes solder joints susceptible to failure caused by electromigration, too. As a result, electromigration in solder joints have started to receive considerable attention in the last several years (Lee and Tu, 2001). Thin films in VLSI circuits are generally pure Al or Cu metals and have considerably higher melting temperatures. Moreover, they have different diffusion boundary conditions then solder joints. Considerably lower melting temperature and higher diffusivity of solder alloys, at room temperature makes them prone to serious damage under a high current density. In addition, having more than one constituent in the alloy makes the diffusion process considerably more complex (Lee and Tu, 2001; Ye et al., 2004).

When a solid conductor is subjected to an electrical potential difference, the current enters from the anode side and travels to cathode side, and the electrons travel from the cathode to the anode side. If the current density is very high (what is high will be qualified latter), the so-called electron-wind transfers part of the momentum to the atoms (or ions) of solid to make the atoms (or ions) move in the direction of the electrons.

* Corresponding author. Tel.: +1 716 645 2114; fax: +1 716 645 3733.
E-mail address: cjb@buffalo.edu (C. Basaran).

0167-6636/$ - see front matter © 2007 Elsevier Ltd. All rights reserved.
doi:10.1016/j.mechmat.2007.06.006

Under high current density, mass accumulation on the anode side, causes local compression and eventually the mass is squeezed out of the surface to form protrusions which are called hillocks and whiskers. When the protrusions contact with a circuit nearby, it causes short circuit failure. While on the cathode side, mass depletion causes tension and vacancy accumulation. Voids nucleating under tensile stress will grow and coalesce until a void forms which leads to an electrical failure. Cathode side failure is the main concern and hence it is under extensive research.

In engineering practice Black (1967) empirical equation is commonly used to predict time to failure of Al or Cu thin films in VLSI circuitry under high current density. Black (1967) equation is an empirical relationship between Median Time to Failure (MTF) and current density as $\mathrm{MTF} \propto j^{-2}$. Constants associated with this empirical formula must be obtained from the thin film that its MTF will be predicted. Different values of current density power exponents have been reported in the literature, ranging from 1 to 15 based on their own experiments (Gleixner et al., 1997). Joule heating effect is believed to be one cause of such discrepancy (Ye et al., 2003c). While accounting for most of the critical parameters of electromigration process, such as, temperature and current density, Black's equation ignores many important factors such as, current crowding, temperature gradient, stress gradient, yield stress, vacancy concentration, material diffusion properties, boundary conditions, and diffusion boundary conditions. As an empirical equation, Black's equation also fails to show completely different failure mechanism exhibited by different diffusion and boundary conditions (Ye et al., 2003b,c,d, 2004).

In order to investigate electromigration failure of solder alloys under various service conditions, computational simulation of damage process is needed. In this paper, this is accomplished by a damage mechanics formulation embedded in a general purpose finite element procedure that can do coupled displacement-diffusion analysis.

2. Damage mechanics formulation

Electromigration is a mass diffusion process that happens under high current density as a result of an exchange of momentum between charge carriers (free electrons) and ions. When the ions move with the free electrons they leave behind vacancies. Although driving force for void growth is well understood, void nucleation due to electromigration has received very little attention (Gleixner et al., 1997). Void nucleation is a complex process, and due to its inherent stochastic nature, the numerical simulation of void nucleation is still quantitatively difficult. Gleixner et al. (1997) and Gleixner and Nix (1996) used thermodynamics and kinematic theory to calculate void nucleation rate. The research results by Gleixner et al. show that void nucleation, due to vacancy condensation is not expected to occur in passivated aluminum thin film interconnect lines unless there are other mechanisms which have extremely low energy barrier. One possibility, as pointed out by Gleixner is flaws at metal/passivation interfaces, where diffusivity is much higher. In Gleixner's calculation, spherical stress is estimated and void nucleation rate is calculated based on spherical stress value. Their assumptions are probably true for passivated thin films in semiconductor devices. Yet, solder joints in electronics operate around at or above $0.6T_\mathrm{m}$ and have large grain boundaries as a result, their diffusivity is very high compared to bamboo structured thin films. Moreover, boundary conditions in solder joints cause serious shear stresses which are negligible in magnitude in VLSI thin film interconnect lines. As Ye et al. (2003b,c,d, 2004) and Lee and Tu (2001) have shown experimentally void condensation happens rather easily in solder joints under high current density.

The void nucleation not only depends on spherical stress (Kircheim, 1992, 1993a), but also on effective stress which is von-Misses stress for metals (Lin and Basaran, 2005). One of the most commonly used models for void nucleation is due to Argon et al. (1975). The decohesion critical stress in Argon Model is defined as a critical combination of two stresses:

$$\sigma_\mathrm{c} = \sigma_\mathrm{m} + \sigma_\mathrm{e} \tag{1}$$

where σ_e is the effective stress, given by

$$\sigma_\mathrm{e} = \sqrt{1/2}\left[(\sigma_1 - \sigma_2)^2 + (\sigma_2 - \sigma_3)^2 + (\sigma_1 - \sigma_3)^2\right]^{1/2} \tag{2}$$

and σ_m is mean spherical stress.

Rice and Tracey (1969) have shown that the rate of growth of a void under triaxial stress state is related to principle strain rate. Argon et al. (1975) and Rice and Tracey (1969) formulations are based

on fracture mechanics of a crack under remote stress field.

In solids undergoing electromigration process the interaction of mass diffusion and confining boundary conditions is the main driving force for void nucleation. For example, if there is no confinement of boundaries, such as the 'drift velocity' measurement in Blech (1976) electromigration experiments, no void nucleation happens, because there is no stress field created due to lack of confinement at the boundaries. This behavior is similar to behavior of an unconfined metal piece subjected to temperature change. It elongates but no stresses field develops at the macro-level. For VLSI interconnect lines, spherical stress level and vacancy concentration level are used as an index for void nucleation. Korhonen et al. (1991, 1992, 1993). Yet von-Misses stresses are not negligible in solder joints undergoing electromigration. Hence, they should be included, because, von-Misses stresses are partly responsible for void nucleation according to Argon et al. (1975). One reason for ignoring von-misses stresses in electromigration process in thin films, has been the fact that boundary conditions in passivated thin films in semiconductor devices are such that shear strain is significantly smaller than spherical strain (Kircheim, 1992, 1993a; Korhonen et al., 1991, 1992, 1993). As pointed out by Goods and Brown (1978), plastic strain plays an important role in void nucleation, such that, there exists a critical strain value for cavity nucleation. Local stress concentrations at the grain boundaries can also decrease incubation time for void nucleation thus accelerating damage process. We assume that, these principles are also valid in electromigration induced stress fields.

In literature, various metrics are used to quantify material degradation under electromigration process. Spherical stress is closely related to void nucleation; therefore the choice of critical spherical stress value as an indicator of void nucleation is commonly used. This concept was adopted by Shatzkes and Lloyd (1986), Trattles et al. (1994) and Park et al. (1999) for thin films. The using critical vacancy concentration as the criterion for void nucleation is the same as using the critical spherical stress value because vacancy concentration and spherical stress are related to each other through thermodynamics equilibrium. Sasagawa et al. (2001) proposed using atomic flux divergence as an damage metric for passivated thin films. Entropy production is used as the damage metric in this research project, which allows accounting for all driving forces operating during electromigration process. But most importantly, using entropy as a metric allows accounting for degradation due to thermomechanical forces, electromigration and thermomigration in the same formulation, without the need for running separate analysis and superposing the damage due to each factor separately. Unified approach simplifies the analysis significantly. Damage evolution model is based on thermodynamics and statistical mechanics. The concept of using entropy as a damage metric has been published previously (Basaran and Yan, 1998; Basaran et al., 2003, 2004; Basaran and Nie, 2004; Gomez and Basaran, 2006; Tang and Basaran, 2003). In here, it is incorporated in to coupled displacement-diffusion based material nonlinear finite element formulation and has been verified against electromigration test data.

Starting from the Helmholtz free energy equation:

$$d\Psi = du - T\,ds - s\,dT \tag{3a}$$

where Ψ is the free energy, u is internal energy, s is entropy and T is the is temperature.

And knowing that in statistical mechanics a precise meaning is given to disorder and expressed by the following relationship

$$S = k \ln w \tag{3b}$$

where k is Boltzmann's constant and w is the disorder parameter. Based on these two principles and laws of thermodynamics the following exponential evolution equation can be derived (Basaran and Yan, 1998; Basaran et al., 2003, 2004; Basaran and Nie, 2004; Gomez and Basaran, 2006; Tang and Basaran, 2003),

$$D = 1 - e^{\frac{-\Delta s}{N_0 k}} \tag{4a}$$

where D is a parameter starts from zero approaches 1 as degradation progresses:

$$\Delta s = \int_{t_0}^{t} \left(\frac{1}{T^2} C|\mathrm{Grad}(T)|^2 + \frac{C_v D_v}{kT^2} \left(Z^* e\rho\vec{j} - f\Omega\nabla\sigma + \frac{Q\vec{\nabla}T}{T} + \frac{kT}{C}\vec{\nabla}C \right)^2 + \frac{1}{T}\boldsymbol{\sigma} : \varepsilon_p \right) dt \tag{4b}$$

where N_0 is the Avogadro's constant, k is Boltzmann's constant, C_v is atomic vacancy concentration, D_v is effective vacancy diffusivity, Z^* is vacancy effective charge number, e is electronic charge of an electron, ρ is metal resistivity, $\vec{j}$ is

current density vector, f is vacancy relaxation ratio, the ratio of the volume of an atom to the volume of a atomic vacancy, Ω is atomic volume, T is absolute temperature (K), $\sigma = \text{trace}(\sigma_{ij})/3$, $\boldsymbol{\sigma}$ is stress tensor and ε_p is the plastic strain rate tensor.

Entropy production based damage evolution model has been successfully implemented to simulate thermomechanical fatigue failure of solder joints and particle filled composites extensively (Basaran and Yan, 1998; Basaran et al., 2004; Basaran and Nie, 2004; Gomez and Basaran, 2005, 2006; Tang and Basaran, 2003; Nie and Basaran, 2007). In here, it is extended to electromigration process and validated for simulating failure of solder joints subjected to electromigration.

3. Formulation

Details of formulation are presented in Nie and Basaran (2007). Because of space limitations only a summary of the formulation are presented below.

3.1. Governing equations

Electromigration is diffusion controlled mass transport process. It is governed by the vacancy conservation equation which is equivalent to mass conservation equation:

$$\int_v \left(C_{v0} \frac{\partial c}{\partial t} + \nabla \cdot \mathbf{q} - G \right) \mathrm{d}V = 0 \tag{5}$$

where C_{v0} is the equilibrium vacancy concentration in the absence of a stress field, c is normalized vacancy concentration and $c = \frac{C_v}{C_{v0}}$, C_v is instantaneous vacancy concentration, t is time, $\mathbf{q}$ is vacancy flux (a vector), G is the vacancy generation/annihilation rate.

The driving forces during electromigration are vacancy concentration gradient, electrical field forces, stress gradient and temperature gradient. Hence, the vacancy flux can be given by Basaran et al. (2003), Lin and Basaran (2005) and Sarychev and Zhinikov (1999):

$$\mathbf{q} = -D_v C_{v0} \left(\nabla c + \frac{Z^* e}{kT} (-\rho \mathbf{j}) c + \frac{c f \Omega}{kT} \nabla \sigma_{\text{spherical}} + \frac{c}{kT^2} Q^* \nabla T \right) \tag{6}$$

where D_v is the effective vacancy diffusivity, $\sigma_{\text{spherical}}$ is spherical part of stress tensor, $\sigma_{\text{spherical}} = \text{trace}(\sigma_{ij})/3$, Q^* is heat of transport, the isothermal heat transmitted by moving the atom in the process of jumping a lattice site less the intrinsic enthalpy.

The stress–vacancy relationship is represented by vacancy generation/annihilation rate which is given by (Sarychev and Zhinikov, 1999):

$$G = -C_{v0} \frac{c - C_{ve}}{\tau_s} \tag{7}$$

where $C_{ve} = \mathrm{e}^{\frac{(1-f)\Omega \sigma_{\text{spherical}}}{kT}}$ is normalized thermodynamic equilibrium vacancy concentration. τ_s is the characteristic vacancy generation/annihilation time.

3.2. Constitutive equation

The stress–strain constitutive model is established as follows:

$$\sigma = C(\varepsilon_{\text{total}} - \varepsilon_{\text{viscoplastic}} - \varepsilon_{\text{electromigration}} - \varepsilon_{\text{thermal}}) \tag{8}$$

where $C = \kappa(1 \otimes 1) + 2\mu\left(I - \frac{1}{3} 1 \otimes 1\right)$, κ is the bulk modulus and μ is the shear modulus:

$$\mathbf{I} = \begin{bmatrix} 1 & 0 & 0 & 0 & 0 & 0 \\ 0 & 1 & 0 & 0 & 0 & 0 \\ 0 & 0 & 1 & 0 & 0 & 0 \\ 0 & 0 & 0 & 0 & 0 & 0 \\ 0 & 0 & 0 & 0 & 0 & 0 \\ 0 & 0 & 0 & 0 & 0 & 0 \end{bmatrix}, \quad \mathbf{1} = \begin{bmatrix} 1 \\ 1 \\ 1 \\ 0 \\ 0 \\ 0 \end{bmatrix}$$

Itemized strain components:

$$\varepsilon_{\text{total}} = \frac{1}{3} \varepsilon_{\text{total}}^{\text{trace}} \cdot \mathbf{1} + \varepsilon_{\text{total}}^{\text{dev}} \tag{9}$$

$$\varepsilon_{\text{viscoplastic}} = \frac{1}{3} \varepsilon_{\text{viscoplastic}}^{\text{trace}} \cdot \mathbf{1} + \varepsilon_{\text{viscoplastic}}^{\text{dev}} = \varepsilon_{\text{viscoplastic}}^{\text{dev}} \tag{10}$$

$$\varepsilon_{\text{electromigration}} = \frac{1}{3} \varepsilon_{\text{electromigration}}^{\text{trace}} \cdot \mathbf{1} + \varepsilon_{\text{electromigration}}^{\text{dev}} = \frac{1}{3} \varepsilon_{\text{electomigration}}^{\text{trace}} \cdot \mathbf{1} \tag{11}$$

$$\varepsilon_{\text{thermal}} = \frac{1}{3} \varepsilon_{\text{thermal}}^{\text{trace}} \cdot \mathbf{1} \tag{12}$$

Substitute Eqs. (9)–(12) into Eq. (8), we obtain:

$$\begin{aligned} \sigma &= \kappa\left(\varepsilon_{\text{total}}^{\text{trace}} - \varepsilon_{\text{electromigration}}^{\text{trace}} - \varepsilon_{\text{thermal}}^{\text{trace}}\right) \cdot \mathbf{1} + 2\mu\left(\varepsilon_{\text{total}}^{\text{dev}} - \varepsilon_{\text{viscoplastic}}^{\text{dev}}\right) \\ \sigma &= \kappa\left(\varepsilon_{\text{total}}^{\text{trace}} - \varepsilon_{\text{electromigration}}^{\text{trace}}\right) \cdot \mathbf{1} + 2\mu\left(\varepsilon_{\text{total}}^{\text{dev}} - \varepsilon_{\text{viscoplastic}}^{\text{dev}}\right) \end{aligned} \tag{13}$$

where $\varepsilon^{\text{trace}}_{\text{electromigration}}$ is defined by following equation (Sarychev and Zhinikov, 1999):

$$\frac{\partial \varepsilon^{\text{trace}}_{\text{electromigration}}}{\partial t} = \Omega C_{v0}(f\nabla \mathbf{q} + f'G) \tag{13a}$$

$$f' = 1 - f$$

According to Eq. (13a), proposed by Sarychev and Zhinikov (1999), it is assumed that when an atom moves under electromigration forces it leaves behind a vacancy. There is a local spherical strain induced at that lattice site due to difference between the volume of an atom and the volume of a vacancy. As a result during electromigration spherical strain happens due to:

(1) Vacancy flux divergence.
(2) Vacancy generation.

Using Eq. (7), we can transform Eq. (13a) into

$$\frac{\partial \varepsilon^{\text{trace}}_{\text{electromigration}}}{\partial t} = \Omega C_{v0}\left(G - f\frac{\partial c}{\partial t}\right) = \Omega C_{v0}\left(\frac{e^{\frac{(1-f)\Omega\sigma_{\text{spherical}}}{kT}} - c}{\tau_s} - f\frac{\partial c}{\partial t}\right) \tag{14}$$

Eqs. (13) and (14) plus J_2 plasticity theory yield the constitutive material behavior, which is introduced during solution of P.D.E. given by Eq. (5).

Tang and Basaran (2001), Kashyap and Murty (1981) and Basaran et al. (2004) developed a visco-plastic flow rule for solder alloys based on Kashyap and Murty (1981) model. In Pb/Sn eutectic solder alloys, grain boundary sliding is the dominant creep mechanism, where primary and steady state creep rate can be modeled by:

$$\dot{\varepsilon}^{\text{vp}}_{ij} = \frac{AD_0Eb}{k\theta}\left(\frac{\langle F\rangle}{E}\right)^n\left(\frac{b}{d}\right)^p e^{-Q/R\theta}\frac{\partial F}{\partial \sigma_{ij}} \tag{15}$$

where A is the dimensionless material parameter to describe the strain rate sensitivity, D_0 is a temperature independent diffusion frequency factor, Q is creep activation energy (J/mol), R is the universal gas constant = 8.314 J/K mol = 8.314 N mm/K mol, θ is absolute temperature (K), E is Young's modulus, b is characteristic length of crystal dislocation (magnitude of Burger's vector), k is Boltzmann's constant, d is average phase ("grain") size, p is phase size exponent, n is stress exponent for plastic deformation rate, where $1/n$ indicates strain rate sensitivity and $e^{\left(-\frac{Q}{R\theta}\right)}$ is the Arrhenius temperature dependency of diffusion coefficient.

Yield function is given by,

$$F = \|\mathbf{S} - \mathbf{X}\| - \frac{2}{3}K(\alpha) \tag{16}$$

$\mathbf{S}$ is the deviatoric stress tensor given by

$$\mathbf{S} = \boldsymbol{\sigma} - \frac{1}{3}\,\text{Tr}(\boldsymbol{\sigma})\mathbf{1} \tag{17}$$

$\mathbf{X}$ is a back stress tensor defining the displacement of the center of the yield surface in the deviatoric stress space.

Isotropic and kinematic hardening laws are given by (Lin and Basaran, 2005; Lubarda and Benson, 2002):

$$\dot{\alpha} = \sqrt{\frac{2}{3}}\gamma \tag{18a}$$

$$\dot{\mathbf{X}} = c_1\dot{\boldsymbol{\varepsilon}}^{\mathbf{p}}_{\mathbf{ij}} - c_2\mathbf{X}\dot{\alpha} \tag{18b}$$

where c_1 is the linear kinematic hardening constant and c_2 is the nonlinear kinematic hardening constant.

$K(\alpha)$ represents the isotropic hardening component defining the radius of the yield surface in stress space. It is a function of the hardening parameter α:

$$K(\alpha) = \sqrt{\frac{2}{3}}Y_0 + R_\infty[1 - e^{-c\alpha}] \tag{19}$$

where Y_0 is the initial yield stress, R_∞ is isotropic hardening saturation value and c is the isotropic hardening rate.

4. Determination of material parameters

4.1. Mechanical material properties (Pb37/Sn63)

Electromigration testing was conducted on flip chip microelectronic package containing eutectic Pb/Sn solder joints. Material properties for this alloy are as follows (see Tables 1–4).

Young's modulus is given by (Basaran et al., 2004):

Table 1
Hardening parameters

Parameter	Value
c_1 (MPa)	13.6
c_2	457.9
C	383.3
R_∞ (MPa)	37.47 − 0.0748T (K)

Table 2
Flow function parameters

Parameter	Value
D_0 (cm^2/s)	0.488
b (Å)	3.18
d (μm)	10.6
n	1.67
p	3.34
Q (kJ/mol)	44.7
A	7.6×10^9

Table 3
Other materials parameters

Ambient temperature	373 K
Vacancy relaxation time (TS)	1.8E−3 s (Sarychev and Zhinikov, 1999)
Effective diffusivity (D)	62.4 μm^2 s^{-1}
Effective charge number (Z^*)	10
Resistivity (ρ)	1.450E−11 μm^3 s^{-3} A^{-2} kg (Pecht et al., 1998)
Average vacancy relaxation ratio (f)	0.6 (Sarychev and Zhinikov, 1999)
Atomic volume of tin (Ω)	2.71E−11 μm^3
Initial vacancy concentration (C_{v0})	1.11E−6 μm^{-3} (Balzer and Sigvaldason, 1979)
Boltzmann constant (AK)	1.38E−11 μm^2 s^{-2} K^{-1} kg^{-1}
Universal gas constant	8.314E−6 μm s^{-2} kg mol^{-1} K^{-1}
Avogadro's constant	6.02E−23 atoms/mol

Table 4
Diffusivity of Pb and Sn

Diffusant	D_l^0 (10^{-5} m^2/s)	Q_l (kJ/mol)	$\delta D_{i/b}^0$ (10^{-15} m^3/s)	$Q_{i/b}$ (kJ/mol)
Pb	1.5	100	7000	77.0
Sn	4.1	99	700,000	84.8

$$E(T) = 62.00 - -0.067T\ (\mathrm{K}) \tag{20a}$$

The yield stress is given by (Basaran et al., 2004):

$$\sigma_Y(T) = 60.069 - 0.140T\ (\mathrm{K}) \tag{20b}$$

4.2. Determination of effective diffusivity

Lattice and grain boundary diffusivities for Pb38/Sn62 are given by Gupta et al. (1998), Mehrer and Seeger (1972) and Decker et al. (1977) as follows.

Where D_l^0 is the lattice diffusivity, $D_{i/b}^0$ is interface/grain boundary diffusivity, δ is grain boundary width, for near eutectic Pb/Sn it is assumed to be 0.5 nm (Gupta, 1997), Q_l is lattice diffusion activation energy and $Q_{i/b}$ is the interface/grain diffusion activation energy.

According to Gupta (1997), effective diffusivity is determined by:

$$D_{\mathrm{Effe}} = D_l + \frac{4\delta D_{b/i}}{L} \tag{21a}$$

where D_l and $D_{b/i}$ temperature dependency follow Arrhenius rate equation given by:

$$D_l = D_l^0 e^{-\frac{Q_l}{kT}}$$
$$D_{b/i} = D_{b/i}^0 e^{-\frac{Q_{b/i}}{kT}} \tag{21b}$$

and L is average grain/phase size, its value is estimated as 2 μm according to Ye et al. (2003a).

Based on the values and relations given above, D_{Effe} for Pb and Sn are:

$$D_{\mathrm{Effe}}^{\mathrm{Pb}} = 2.307 \times 10^{-16}\ (\mathrm{m}^2/\mathrm{s})$$
$$D_{\mathrm{Effe}}^{\mathrm{Sn}} = 1.864 \times 10^{-15}\ (\mathrm{m}^2/\mathrm{s}) \tag{22}$$

respectively, for Pb and Sn at 373 K.

The equilibrium vacancy concentration at a stress free state is reported as $C_{v0}/C_a = 3 \times 10^{-5}$ by Balzer and Sigvaldason (1979) with $C_a = 3.69 \times 10^{22}$ cm^{-3} for pure tin.

Based on the relation of vacancy diffusivity and atomic diffusivity (Clement and Thompson, 1995)

$$D_a C_a = D_v C_v \tag{23}$$

at a stress free state, D_v can be obtained as

$$D_v = 62.14\ (\mu\mathrm{m}^2/\mathrm{s}) \tag{24}$$

5. Numerical simulation

5.1. Samples structure

The experimental tests of electromigration were conducted by Ye et al. (2003b,c,d) on actual flip chip modules. The schematic cross-sections of the test module and a solder joint are shown in Fig. 1. The under bump metallization (UBM) on the silicon die side is electroless nickel (Ni). The diameter of the solder (Pb37/Sn63) joint is around 140 μm and the height is about 100 μm. The solder joints are encapsulated in the underfill between the silicon die and PCB. Copper (Cu) plate surfaces are plated with a nickel barrier layer.

5.2. Boundary conditions and current crowding

For diffusion, blocking boundary conditions are used at the top and bottom. The reason for using blocking diffusion boundary conditions is the fact

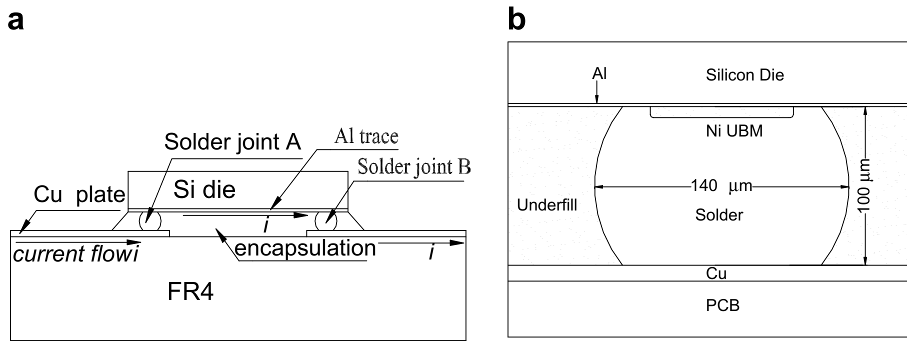

Fig. 1. (a) Cross-section of the test module; (b) cross-section of a solder joint (Ye et al., 2003b).

that there is a diffusion barrier layer of electroless Ni on the copper metallization.

Electrical current field in solder joints is not uniform. Due to difference in thickness of the thin layer of aluminum trace on the Si die side and solder joints side, the current density in the thin aluminum trace is at least one order of magnitude larger than the current density in the solder joints. When the electrical current enters solder joint from silicon die side, at the junction interface, there will be a current crowding, where current density in the solder joint is much higher than the average nominal value. In order to account for current crowding effect, a current density field profile is obtained by electromagnetic analysis on the test vehicle shown in Fig. 1, using ABAQUS general purpose finite element analysis package. The results from the electro-magnetic field analysis are used as input for the next step electromigration simulations. Five different current density values are used in simulations ranging from 0.2×10^4 to 1.0×10^4 A/cm^2. (These are the average nominal current density values assuming uniform current distribution in a solder joint.) The electrical potential gradient analysis results for the solder joint are shown in Fig. 2. It is clear that current density at the corner of the solder joint is very high compared to nominal average value.

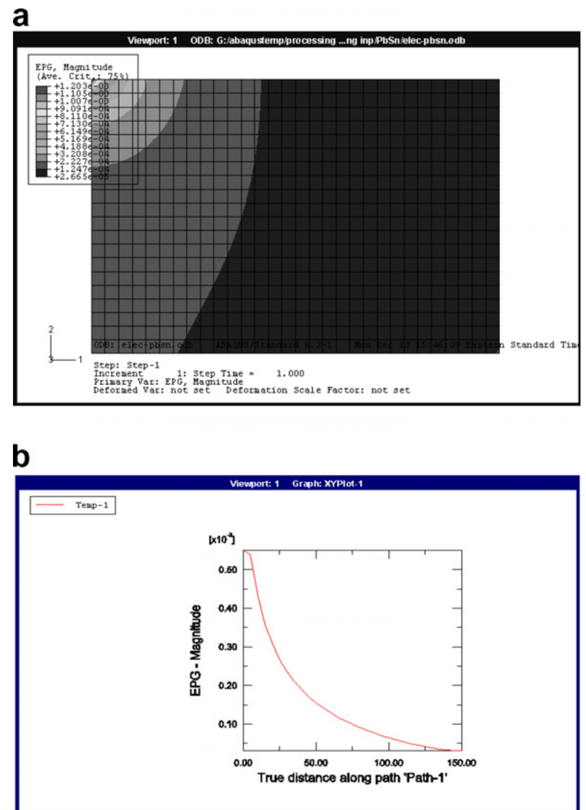

Fig. 2. Current field simulation: (a) contour; (b) distribution along the upper edge (EPG: Electrical Potential Gradient).

5.3. Simulation results

Simulation results for the nominal current density of 0.2×10^4 A/cm^2 are shown in Fig. 3. The normalized atomic vacancy concentration and spherical stress distribution are shown in Fig. 3a and b, respectively. The upper left corner has the largest value of vacancy concentration and spherical stress (positive value is tension). As expected, current crowding point has the highest vacancy concentration. On the other hand, the lower right corner is a compression zone. Plastic shear strain and equivalent plastic strain distribution after 100 h of current stressing are shown in Fig. 3c and d, respectively. There are two concentration areas for plastic shear stain and equivalent plastic strain. One is at the upper boundary close to the left side

and the other is at middle of left boundary. Both are due to interaction of the displacement boundary conditions and deformation caused by vacancy generation. Damage distribution, as defined by Eq. (4a), is shown in Fig. 3e. In the damage calculation, the damage value in the compression zone is set to be zero, because in experiments failure due to electrical disconnect always happens in the tension region (cathode) where voids develop. In Fig. 3e, damage distribution shows a profile similar to equivalent plastic strain and plastic shear strain. This means that the damage contribution, according to Eq. (4), from plastic work is the largest.

The total atomic flux divergence is the ratio between change of atomic concentration and original atomic concentration. The total atomic flux divergence distribution is shown in Fig. 3f. The most critical damage area is in the upper edge, which is near the silicon die side UBM and solder joint junction. In order to identify the most critical location in the solder joint, normalized vacancy concentration, damage and total atomic divergence

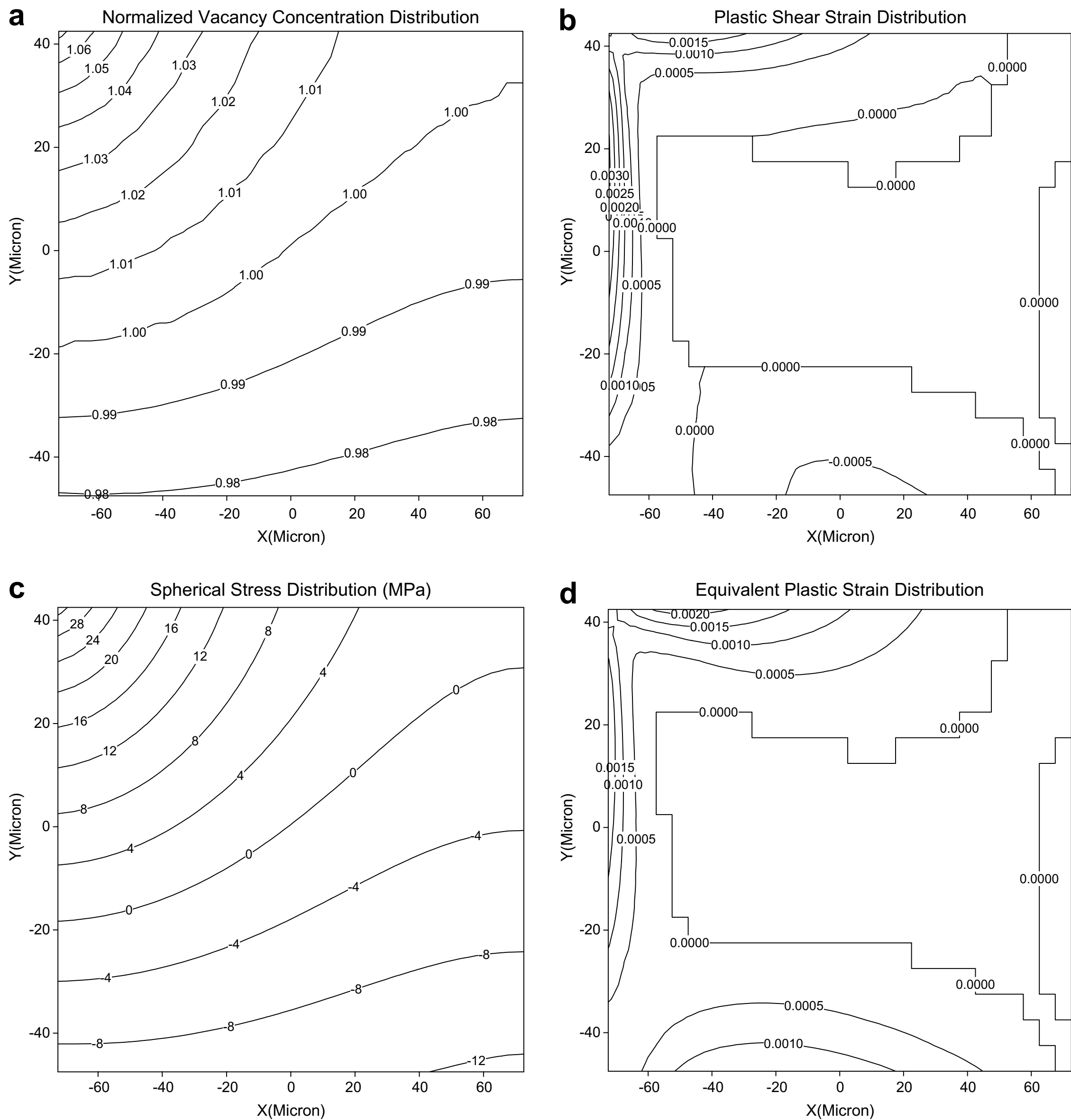

Fig. 3. Simulation result at 100 h for current density of 0.2×10^4 A/cm^2.

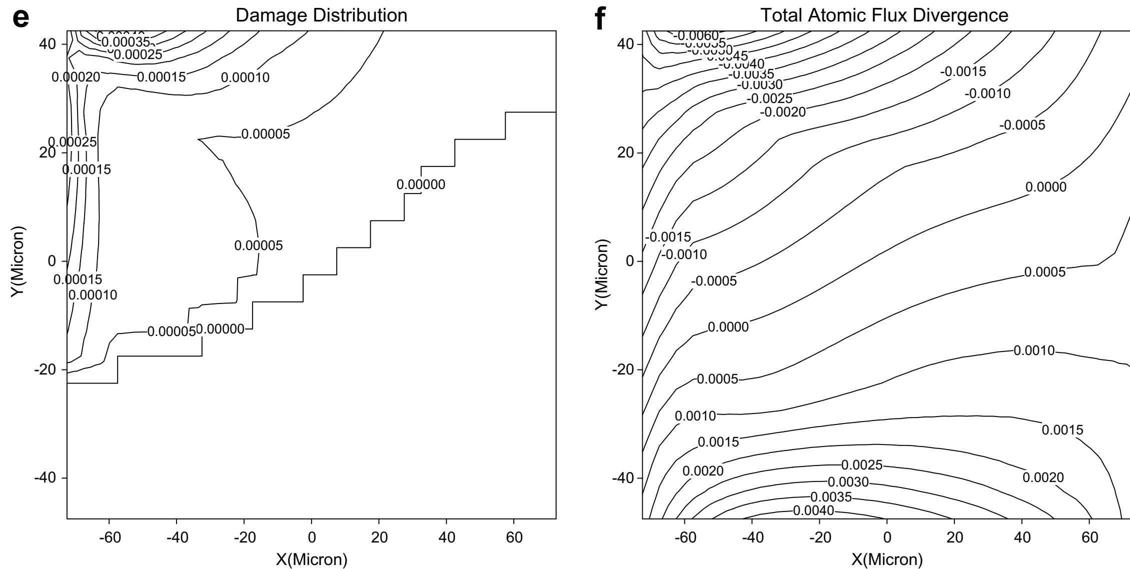

Fig. 3 (*continued*)

flux results for the upper edge of the solder joint are shown in Fig. 4. The most critical location is not at the corner but a little bit away form the corner position. This critical location is studied in depth for different current density levels.

Fig. 5 shows the normalized vacancy concentration evolution at different current density levels at the critical point in the solder joint. The normalized vacancy concentration level will reach stable position at different times for different current density levels. Damage evolution for the most critical point for different current density levels is shown in Fig. 6. Fig. 6a shows the damage evolution for two smaller current density levels of 0.2×10^4 and 0.4×10^4 A/cm^2. Fig. 6b shows the results for three higher current density levels of 0.6×10^4, 0.8×10^4 and 1.0×10^4 A/cm^2. At low current density levels, the damage reaches an asymptotic steady state level rapidly due to counterbalancing spherical stress gradient and concentration gradient. At higher current density levels, the counterbalancing forces (namely spherical stresses and concentration gradient) cannot resist the electron wind force, after the counter balance forces reach a maximum value, damage accumulation continues to increase until failure. At this stage (after electrical field forces have overcome counter acting forces) damage accumulation rate is constant as seen in Fig. 6b. The steady state damage accumulation rate can be verified by vacancy flux at the critical point of a solder joint, which is shown in Fig. 7. At low current density levels, the vacancy flux stops after 100 h of current stressing. For higher current density values (above 0.6×10^4 A/cm^2) levels, the vacancy flux reaches a steady state value but does not become zero after 100 h of current stressing.

The total atomic flux divergence results at the critical point are shown in Fig. 8a and b. The total atomic flux divergence is a mass depletion ratio. It is commonly interpreted as a physical void ratio. At highest current density level after 100 h of simulation, the total atomic divergence is around 70%, Fig. 8b. This means the mass depletion ratio is very high and void nucleation will occur well before that. Comparing the damage evolutions shown in Fig. 6a and b, and the total atomic flux divergence time history evolutions shown in Fig. 8a and b, it is obvious that, they are very similar. Since the total atomic flux divergence has a direct physical meaning (mass depletion ratio), this proves that our entropy production based damage formulation, given in Eq. (4a), is very successful in representing the physical damage evolution. Yet, we need to identify a critical damage value to be able to use this damage evolution model for mean time failure prediction. This task is tackled in the following pages.

Fig. 9 shows the nonlinear stress strain relationship at the critical point for three high current density levels. The nonlinear isotropic hardening effect can be clearly seen from Fig. 9. Due to difference in electromigration driving forces, larger forces (which happen due to larger current density) create

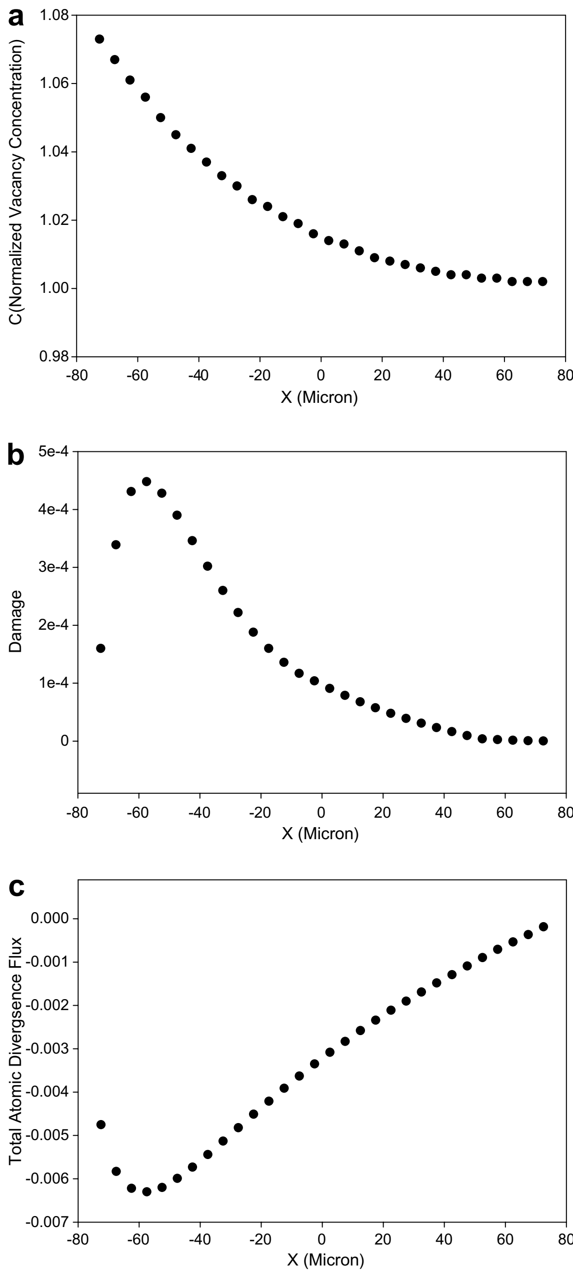

Fig. 4. Simulation results for upper edge at 100 h for current density at $0.2 \times 10^4 A/cm^2$.

a larger strain rate, and that rate sensitivity can be clearly seen in Fig. 9.

In order to determine the incubation time to reach a critical damage value for void nucleation, linear regression is used to determine the time to failure as a function of damage. Incubation time is commonly used as a criterion for failure (Lin et al., 2005). At higher current density values dam-

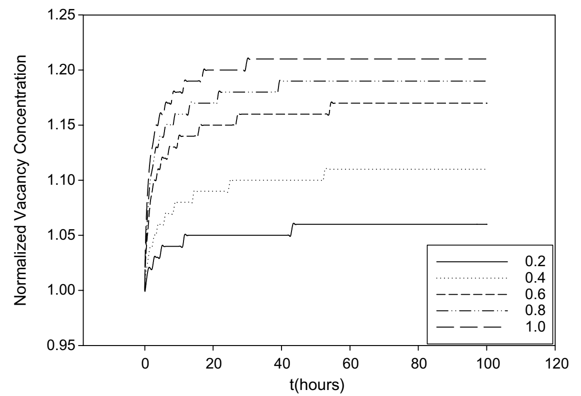

Fig. 5. Normalized vacancy concentration evolution at different current density levels.

age evolves linearly with time at later stages, a linear regression is reasonably accurate. According to the 95% confidence level linear regression results, the time needed to reach different critical damage values for three different current density levels (low current

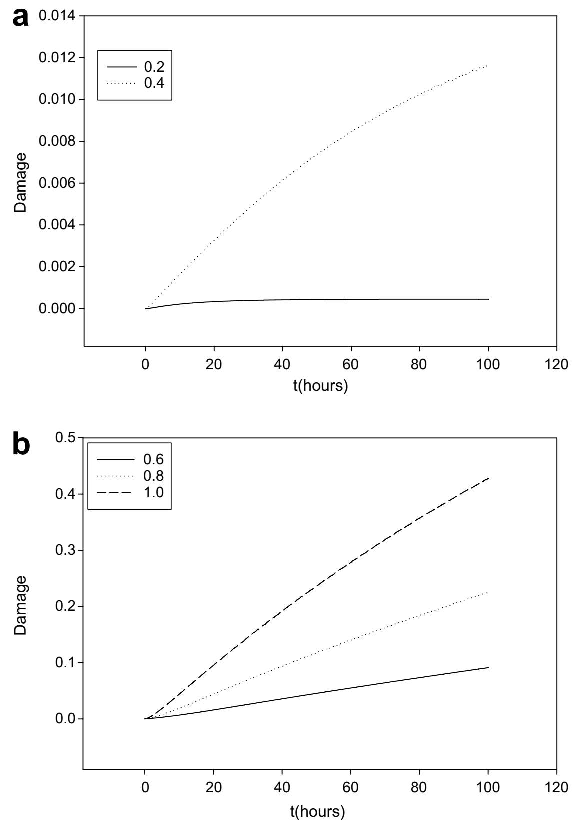

Fig. 6. Damage evolution for 100 h of current stressing for different current density levels.

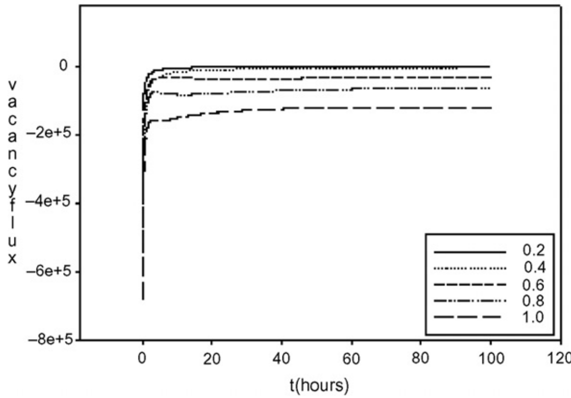

Fig. 7. Vacancy flux time history at the critical point of the solder joint for different current density levels.

density is not considered) is fitted, the function has the following form

$$t = A \cdot \text{Damage} \tag{25}$$

Using simulation results presented in Fig. 6 three different values of parameters A are obtained 1098.2, 435.33 and 222.41 for three different current density levels of 0.6×10^4, 0.8×10^4 and 1.0×10^4 A/cm^2, respectively. The calculated value of t is in hours. Comparing the parameter A value with the corresponding current density value, the time to reach critical damage is proportional to j^{-3} according to the simulation results.

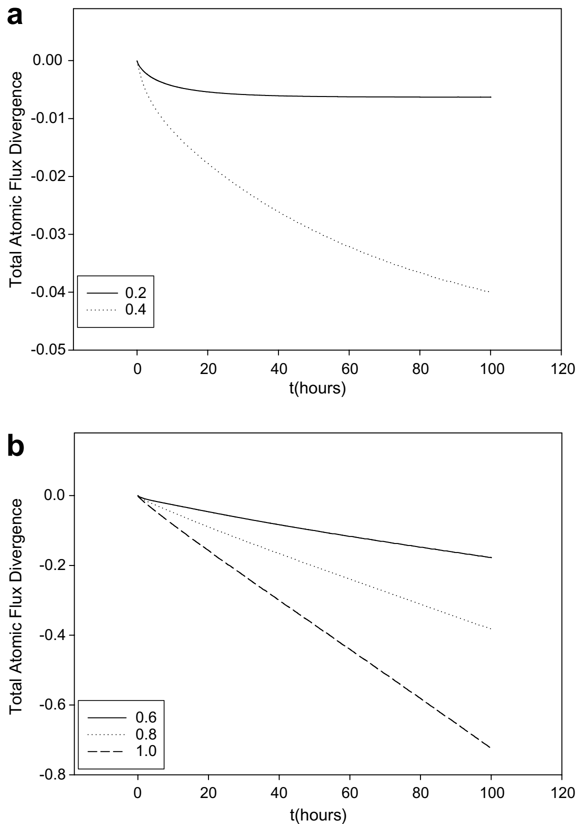

Fig. 8. Total atomic flux divergence at the critical point of solder joint for different current densities.

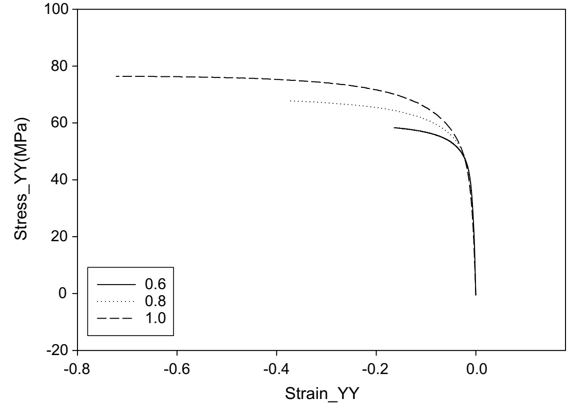

Fig. 9. Stress and strain evolution.

5.4. Validation of the damage evolution model

The test data used for validating the model is presented in Table 5. In order to utilize the experimental data for verification of the damage model and to determine the damage evolution time history, a two parameter exponential function fit is conducted using the Table Curve 3D software package. The following exponential function fits the test data given in Table 5:

$$t = \frac{a}{j^3} \exp\left(\frac{b}{T}\right) \tag{26}$$

where a and b are parameters to be determined by the least square method and t is time to failure, j (10^4 A/cm^2) is the current density, and T is temperature (K). Utilizing the test data given in Table 5, the values of a and b are determined to be 3.824E−4 and 4961.4, respectively. The detailed results are listed in fifth column of Table 5.

Now, using this test data and its polynomial representation given in Eq. (26), we can verify our model. According to Eq. (26), at a temperature of 373 K and at current density levels of 0.6×10^4, 0.8×10^4 and 1.0×10^4 A/cm^2, the time to failure would be 1058.7, 446.6 and 228.7 h, respectively. In Eq. (25) (which was obtained by computer simulation results), if we choose a critical damage value of 1.0, the time to failure for these three current

Table 5
Test data and regression values, after Ye et al. (2003b)

Test module	Current density (10^4 A/cm^2)	Temperature (K)	Time to failure (h)	Eq. (26), predicted time to failure	Residue	Residue (%)
1	1.2	428	26	23.952088	2.047912	7.876584
2	1.13	413	61	43.70169	17.29831	28.35789
3	0.96	423	61	53.651438	7.348562	12.04682
4	0.72	393	256	311.34605	−55.3461	−21.6196
5	0.64	403	323	324.08069	−1.08069	−0.33458
6	0.62	373	960	959.50163	0.498372	0.051914

densities are 222.41, 435.33 and 1098.2 h, respectively. It is very obvious that simulation predictions are very close to the experimental data values. Assuming a value of 1 for critical damage parameter is reasonable, since the damage evolution function given in Eq. (4a) start from zero and goes to 1 as the final value. When the damage value reaches 1, the material loses the ability of sustain any load or current and results in total failure. An engineer could use a smaller critical damage value in order to introduce a factor of safety in to the design.

6. Conclusions

A damage evolution model based on thermodynamics has been proposed and implemented into finite element procedure for prediction of nanoelectronics solder joint's time to failure under high current density. Comparison with test data verifies the effectiveness of the proposed model.

According to computer simulations and experimental results, at current density levels below 0.6×10^4 A/cm^2, the time to failure increases significantly and TTF does not follow the same trend as higher current densities. This is because of the fact that the counter-balancing forces can effectively eliminate the electromigration driving forces and create a stabilized neutral state where electromigration cannot induce any additional damage beyond the initial stage. Above 0.6×10^4 A/cm^2 current density, time until failure is inversely proportional to the cubic power of the current density (nominal current density value not of the current crowding point).

Simulations indicate that current crowding is a dominant factor that has a serious influence on the damage evolution induced. Eliminating or reducing current crowding would significantly increase the time to failure. In order to prove this latter point the following exercise was done. A uniform current density of 0.8×10^4 A/cm^2 (with no current crowding) was applied to the same model. A comparison of the damage evolution and stress–strain relations for uniform current density case and current crowding case are shown in Fig. 10. Although the nominal current density is the same in both cases, the damage evolution in the current crowding case is much faster than the uniform current density case. The stress–strain curve clearly shows a much higher stress and strain level for current crowding case. The rate sensitivity of the solder material is also exhibited clearly.

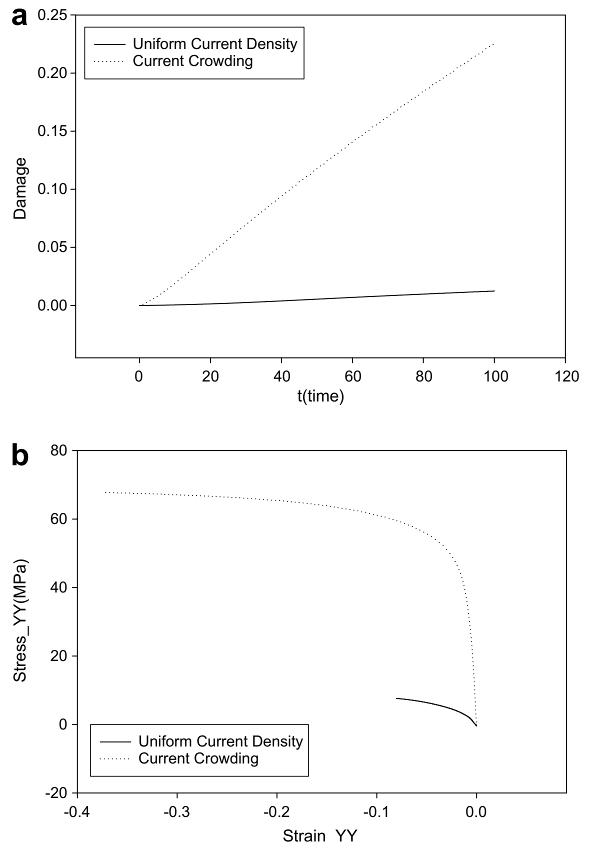

Fig. 10. Comparison between current crowding and uniform current density.

Current crowding greatly depends on the thickness of the Under Bump Metallization (UBM) on the silicon die side. If the thickness of the UBM is increased, the effect of current crowding will be greatly minimized, as a result of the reduction in the difference between the current density in the UBM and the current density in the solder joint.

The damage formulation proposed here is a powerful tool and it can be used to predict time to failure in solder joints under high current density, as in nanoelectronics and next generation power electronics.

Acknowledgement

This research project is sponsored by the US Navy Office of Naval Research Advanced Electrical Power Systems Program under the direction of Mr. Terry Ericsen.

References

Argon, A.S., Im, J., Safoglu, R., 1975. Cavity formation from inclusions in ductile fracture. Metallurgical Transactions A-Physical Metallurgy & Materials Science 6A, 825–837.

Balzer, R., Sigvaldason, H., 1979. Equilibrium vacancy concentration measurements on tin single crystals. Physica Status Solidi B: Basic Research 92 (1), 143–147.

Basaran, C., Nie, S., 2004. An irreversible thermodynamic theory for damage mechanics of solids. International Journal of Damage Mechanics 13 (3), 205–224.

Basaran, C., Yan, C.Y., 1998. A thermodynamic framework for damage mechanics of solder joints. Transactions of ASME, Journal of Electronic Packaging 120 (4), 379–384.

Basaran, C., Lin, M., Ye, H., 2003. A thermodynamic model for electrical current induced damage. International Journal of Solids and Structures 40 (26), 7315–7327.

Basaran, C., Tang, H., Nie, S., 2004. Experimental damage mechanics of microelectronics solder joints under fatigue loading. Mechanics of Materials 36, 1111–1121.

Black, J.R., 1967. Mass transport of aluminum by momentum exchange with conducting electrons. In: Proceedings of the Sixth Annual Symposium on Reliability Physics IEEE Cat. 7-15C58, pp. 148–159.

Blech, I.A., 1976. Electromigration in thin aluminum films on titanium nitride. Journal of Applied Physics 47 (4), 1203–1208.

Clement, J.J., Thompson, C.V., 1995. Modeling electromigration-induced stress evolution in confined metal lines. Journal of Applied Physics 78 (2), 900–904.

Decker, D.L., Weiss, J.D., Vanfleet, H.B., 1977. Diffusion of Sn in Pb to 30 kbar. Physical Review B (Solid State) 16 (6), 2392–2394.

Gleixner, R.J., Nix, W.D., 1996. An analysis of void nucleation in passivated interconnect lines due to vacancy condensation and interface contamination. In: Materials Reliability in Microelectronics VI, San Francisco, CA, April 8–12, 1996, pp. 475–480.

Gleixner, R.J., Clemens, B.M., Nix, W.D., 1997. Void nucleation in passivated interconnect lines: effects of site geometries, interfaces, and interface flaws. Journal of Materials Research 12 (8), 2081–2090.

Gomez, J., Basaran, C., 2005. A thermodynamics based damage mechanics constitutive model for low cycle fatigue analysis of microelectronics solder joints incorporating size effects. International Journal of Solids and Structures 42 (13), 3744–3772.

Gomez, J., Basaran, C., 2006. Damage mechanics constitutive model for Pb/Sn solder joints incorporating nonlinear kinematic hardening and rate dependent effects using a return mapping algorithm. Mechanics of Materials 38, 585–598.

Goods, S.H., Brown, L.M., 1978. The nucleation of cavities by plastic deformation. Acta Materialia 27, 1–15.

Gupta, D., 1997. Diffusion process in lead based solders used in microelectronic industry. Design & Reliability of Solders and Solder Interconnection, 59–64.

Gupta, D., Vieregge, K., Gust, W., 1998. Interface diffusion in eutectic Pb–Sn solder. Acta Materialia 47 (1), 5–12.

Kashyap, B.P., Murty, G.S., 1981. Experimental constitutive relations for the high temperature deformation of a Pb–Sn eutectic alloy. Materials Science and Engineering 50 (2), 205–213.

Kircheim, R., 1992. Stress and electromigration in Al-lines of integrated circuits. Acta Metallurgica et Materiala 40 (2), 309–323.

Kircheim, R., 1993. Modelling electromigration and induced stresses in aluminum lines. In: Proceedings of the Materials Research Society Symposium, vol. 309, pp. 101–110.

Korhonen, M.A., Paszkiet, C.A., Li, C.Y., 1991. Mechanism of thermal stress relaxation and stress-induced voiding in narrow aluminum based metallization. Journal of Applied Physics 69 (12), 8083–8091.

Korhonen, M.A., Borgesen, P., Li, C.Y., 1992. Mechanism of stress-induced electromigration induced damage in passivated narrow metallizations on rigid substrates. MRS Bulletin 17 (7), 61–68.

Korhonen, M.A., Borgesen, P., Tu, K.N., Li, C.Y., 1993. Stress evolution due to electromigration in confined metal lines. Journal of Applied Physics 73 (8), 3790–3799.

Lee, T.Y., Tu, K.N., 2001. Electromigration of eutectic SnPb and SnAg3.8Cu0.7 flip chip solder bumps and under-bump metallization. Journal of Applied Physics 90 (9), 4502–4508.

Lin, M., Basaran, C., 2005. Electromigration induced stress analysis using fully coupled mechanical and diffusion finite element analysis with non linear material properties. Computational Materials Science 34/1, 82–98.

Lin, Y.H., Hu, Y.C., Tsai, C.M., Kao, C.R., Tu, K.N., 2005. In situ observation of the void formation-and-propagation mechanism in solder joints under current-stressing. Acta Materialia 53 (7), 2029–2035.

Lubarda, V.A., Benson, D.J., 2002. On the numerical algorithm for isotropic–kinematic hardening with the Armstrong–Frederick evolution of the back stress. Computer Methods in Applied Mechanics and Engineering 191 (33), 3583–3596.

Mehrer, H., Seeger, A., 1972. Analysis of the pressure dependence of self-diffusion with applications to vacancy properties in lead. Crystal Lattice Defects 3 (1), 1–12.

Nie, S., Basaran, C., 2007. A thermodynamic based damage mechanics model for particulate composites. International Journal of Solids and Structures 44, 1099–1114.

Park, Y.-J., Vaibhav, K.A., Carl, V.T., 1999. Simulations of stress evolution and the current density scaling of

electromigration-induced failure times in pure and alloyed interconnects. Journal of Applied Physics 85 (7), 3546–3555.

Pecht, M.G., Agarwal, R., McCluskey, P., Dishong, T., Javadpour, S., Mahajan, R., 1998. Electronic Packaging Materials and Their Properties. CRC Press, New York.

Rice, J.R., Tracey, D.M., 1969. On the ductile enlargement of voids in triaxial stress fields. Journal of Mechanics and Physics of Solids 17, 201–217.

Sarychev, M.E., Zhinikov, Yu.V., 1999. General model for mechanical stress evolution during electromigration. Journal of Applied Physics 86 (6), 3068–3075.

Sasagawa, K., Hasegawa, M., Naito, K., Saka, M., Abe, H., 2001. Effects of corner position and operating condition on electromigration failure in angled bamboo lines without passivation layer. Thin Solid Films 401 (1–2), 255–266.

Shatzkes, M., Lloyd, J.R., 1986. A model for conductor failure considering diffusion concurrently with electromigration resulting in a current exponent of 2. Journal of Applied Physics 59 (11), 3890–3893.

Tang, H., Basaran, C., 2001. Influence of microstructure coarsening on thermomechanical fatigue behavior of Pb/Sn eutectic solder joints. International Journal of Damage Mechanics 10 (3), 235–255.

Tang, H., Basaran, C., 2003. A damage mechanics based fatigue life prediction model. Transactions of ASME, Journal of Electronic Packaging 125 (1), 120–125.

Trattles, J.T., O'Neill, A.G., Mecrow, B.C., 1994. Computer simulation of electromigration in thin-film metal conductors. Journal of Applied Physics 75 (12), 7799–7804.

Ye, H., Basaran, C., Hopkins, D., 2003a. Pb phase coarsening in eutectic Pb/Sn flip chip solder joint under electric current stressing. International Journal of Solids and Structures.

Ye, H., Basaran, C., Hopkins, D., 2003b. Damage mechanics of microelectronics solder joints under high current densities. International Journal of Solids and Structures 40 (15), 4021–4032.

Ye, H., Basaran, C., Hopkins, D., 2003c. Thermomigration in Pb–Sn solder joints under Joule heating during electric current stressing. Applied Physics Letters 82 (8), 1045–1047.

Ye, H., Basaran, C., Hopkins, D., 2003d. Mechanical degradation of solder joints under current stressing. International Journal of Solids and Structures 40 (26), 7269–7284.

Ye, H., Basaran, C., Hopkins, D.C., 2004. Mechanical implications of high current densities in flip–chip solder joints. International Journal of Damage Mechanics 13 (4), 335–345.